

Structural stability and properties of Li_2XN_6 (X = Be, Mg, Ca) ternary nitrides

Rui Wang(王睿), Cai-Zi Zhang(张才姿), Qi-Wen Jiang(蒋其雯), En-Yu Wang(王恩宇), Jie Wei(魏杰), and Hong-Yang Zhu(祝洪洋)

Citation: Chin. Phys. B, 2026, 35 (**3**): 036201. DOI: 10.1088/1674-1056/ae1f03
http://cpb.iphy.ac.cn; http://iopscience.iop.org/cpb

What follows is a list of articles you may be interested in

Theoretical investigation on the H sublattice in CaH_6 and energetic performance

Zhihong Huang(黄植泓), Nan Li(李楠), Jun Zhang(张俊), Xiuyuan Li(李修远), Zihuan Peng(彭梓桓), Chongwen Jiang(江崇文), and Changqing Jin(靳常青)

Chin. Phys. B, 2025, 34 (**8**): 086202. DOI: 10.1088/1674-1056/ade1c3

A novel metastable structure and superconductivity of hydrogen-rich compound CdH_6 under pressure

Yan Yan(闫岩), Chengao Jiang(蒋成澳), Wen Gao(高稳), Rui Chen(陈蕊), Xiaodong Yang(杨晓东), Runru Liu(刘润茹), Lihua Yang(杨丽华), and Lili Wang(王丽丽)

Chin. Phys. B, 2025, 34 (**8**): 086201. DOI: 10.1088/1674-1056/add902

Band gap engineering and vibrational properties of van der Waals semiconductor $ZnPSe_3$ under compression

Rouqiong Su(苏柔琼), Yuying Li(李玉莹), Chunhua Chen(陈春华), Yifang Yuan(袁亦方), and Haizhong Guo(郭海中)

Chin. Phys. B, 2025, 34 (**6**): 066205. DOI: 10.1088/1674-1056/adcaa2

Structural regulation and optical behavior of zero-dimensional Cu(I)-based organometallic halides under pressure

Runnan Ye(叶润楠), Jingtian Wang(王敬天), Jiayi Yang(杨佳毅), Xuchen Wang(王旭晨), Junce Lei(雷钧策), Wenya Zhao(赵文雅), Yufan Meng(孟雨凡), Guanjun Xiao(肖冠军), and Bo Zou(邹勃)

Chin. Phys. B, 2025, 34 (**6**): 066204. DOI: 10.1088/1674-1056/adc193

Stoichiometric change and solid decomposition in Ca-S compounds under high pressure

Yang Lv(吕阳), Jian-Fu Li(李建福), Zhao-Bin Zhang(张钊彬), Yong Liu(刘勇), Jia-Nan Yuan(袁嘉男), Jia-Ni Lin(林佳妮), and Xiao-Li Wang(王晓丽)

Chin. Phys. B, 2025, 34 (**4**): 046202. DOI: 10.1088/1674-1056/adb38e

---

SPECIAL TOPIC — Structures and properties of materials under high pressure

Structural stability and properties of Li_2XN_6 (X = Be, Mg, Ca) ternary nitrides

Rui Wang(王睿)[1], Cai-Zi Zhang(张才姿)[1], Qi-Wen Jiang(蒋其雯)[1], En-Yu Wang(王恩宇)[1,†], Jie Wei(魏杰)[1,‡], and Hong-Yang Zhu(祝洪洋)[1,2,§]

[1] *School of Physics and Electronic Engineering, Linyi University, Linyi* 276000, *China*

[2] *Department of Physics and Engineering Physics, The University of Tulsa, Tulsa, Oklahoma* 74104, *United States*

(Received 21 October 2025; revised manuscript received 11 November 2025; accepted manuscript online 13 November 2025)

Polynitrogen compounds have attracted significant interest as high-energy-density materials (HEDMs), while their extreme synthesis and preservation conditions hinder their practical applications. Metal incorporation into nitrogen frameworks has emerged as an effective strategy to reduce the synthesis and stabilization pressures of polynitrogen compounds. In this study, we theoretically predict three novel lithium-alkaline-earth metal nitrides: cage-like R-3m Li_2BeN_6, cage-like R32 Li_2MgN_6, and layered P-62m Li_2CaN_6. Phonon spectrum calculations indicate that R-3m Li_2BeN_6 remains stable between 50–100 GPa, and that R32 Li_2MgN_6 and P-62m Li_2CaN_6 are stable under ambient pressure conditions. *Ab initio* molecular dynamics (AIMD) simulations indicate that R-3m Li_2BeN_6, R32 Li_2MgN_6, and P-62m Li_2CaN_6 remain thermally stable up to 2500 K, 1500 K, and 500 K, respectively. Electronic band structure analysis indicates that R-3m Li_2BeN_6 is semiconducting, while R32 Li_2MgN_6 and P-62m Li_2CaN_6 exhibit metallic characteristics. These differences arise from variations in cation radius and electronegativity, which influence the electron distribution within the lattice. The cage-like R-3m Li_2BeN_6 with a chair-shaped N_6^{6-} ring exhibits an energy density of 4.38 kJ/g upon decomposition into Li_3N, Be_3N_2, and N_2, indicating its potential as an HEDM. These findings not only highlight the role of metal insertion in stabilizing polymeric nitrogen at lower pressures but also provide novel guidance for the design of energetic materials.

Keywords: high pressure, Li_2XN_6 (X = Be, Mg, Ca), density functional theory, high-energy-density materials

PACS: 62.50.–p, 82.40.Fp, 91.60.Gf

DOI: 10.1088/1674-1056/ae1f03 **CSTR:** 32038.14.CPB.ae1f03

1. Introduction

Polymeric nitrogen has been widely investigated as a promising high-energy-density materials (HEDMs). Its high energy density is attributed to the differences in bond energies among various nitrogen bonds. There are three types of chemical bonds between nitrogen atoms: single bonds N–N, double bonds N=N, and triple bonds N≡N, with bond energies of 160 kJ/mol, 418 kJ/mol, and 954 kJ/mol, respectively.[1] Due to the significant energy difference between N–N and N≡N, a substantial amount of energy is released when single-bonded nitrogen compounds convert into triple-bonded nitrogen molecules, surpassing that of any known non-nuclear explosive reactions.[2] Since the first discovery of single-bonded cubic-gauche nitrogen (cg-N) in 2001,[3] the exploration of pure nitrogen materials has attracted considerable attention. The discovery of a pure nitrogen phase stable at ambient pressure and with an energy density of approximately 11.31 kJ/g has further stimulated exploration of high-energy-density polynitrogen compounds under ambient conditions.[4] However, achieving a pure polymeric nitrogen structure with higher stability and milder synthesis conditions remains a challenge.

Theoretical and experimental studies have demonstrated that doping with metal elements facilitates the formation of polymeric nitrogen compounds at pressures significantly lower than those required for pure polymeric nitrogen. Metal dopants not only induce a chemical pre-pressure effect but also donate electrons to the nitrogen framework.[5] This electron transfer enhances the ionicity of chemical bonds and optimizes bonding characteristics.[6] These two effects complement each other, thereby reducing the synthesis pressure and enhancing the structural stability of polymeric nitrogen. In recent years, several nitrogen-rich HEDMs have been reported, including Be–N,[7–11] Mg–N,[12–14] Al–N,[6,15–18] Fe–N,[19–21] Cu–N,[22–24] Zn–N,[25–28] Hg–N,[29] Ta–N,[30] and W–N.[31] Research findings indicate the presence of diverse nitrogen species in these systems, ranging from small units such as N_3 to larger clusters up to N_{13}. Under high-pressure conditions, various nitrogen molecular or ionic configurations have been identified, including N_4 chains, N_5 molecules, zigzag nitrogen chains, extended chains linked by folded N_6 rings, as well

†Corresponding author. E-mail: wangenyu@lyu.edu.cn

‡Corresponding author. E-mail: weijie@lyu.edu.cn

§Corresponding author. E-mail: hongyang-zhu@utulsa.edu

© 2026 Chinese Physical Society and IOP Publishing Ltd. All rights, including for text and data mining, AI training, and similar technologies, are reserved.

as N_{10} and N_{18} rings. For instance, in LiN_3,[32] NaN_3,[33] and KN_3,[34] applied pressure induces a structural evolution in which initially linear N_3 units transform into hexagonal N_6 rings, eventually forming extended polymeric nitrogen networks. As these structures, including LiN_3,[32] and analogous compounds, contain stabilized N_6 rings, they exhibit potential for application as HEDMs. Nevertheless, the successful synthesis of such compounds remains limited.

Based on the concept of the inductive effect proposed by Etourneau *et al.*,[35] the binding energy of these compounds primarily arises from the electrostatic interaction between anions and cations, which stabilizes the metal–nitrogen bonds in ternary and higher-order nitrides. Notably, metal nitrides are not necessarily ionic compounds but may exhibit distinct valence states and bonding behaviors, reflecting the complexity of chemical bonding in such systems. According to this theory, the introduction of an additional metal element into binary metal nitrides enables the formation of novel ternary polynitrogen compounds. The complementary electronic properties of the two metals allow more efficient and balanced charge transfer in bimetal-doped ternary compounds. Consequently, enhanced charge transfer improves the stability of the polymeric nitrogen component. The compounds LiBeN,[36] LiMgN,[37] and LiCaN[38] have been successfully synthesized experimentally, providing direct support for the feasibility of bimetal-doped nitrogen systems, although the form of nitrogen differs. In LiXN, nitrogen exists as isolated N^{3-} anions, whereas in Li_2XN_6, nitrogen may exist as N clusters. Therefore, by increasing the nitrogen stoichiometry in the LiXN (X = Be, Mg, Ca) system, the synthesis of stable high-energy-density Li_2XN_6 compounds is feasible.

In this study, we predict *R*-3*m* Li_2BeN_6, *R*32 Li_2MgN_6, and *P*-62*m* Li_2CaN_6 using an efficient and unbiased automated structure search method. Among them, *R*-3*m* Li_2BeN_6 features a chair-like N_6^{6-} ring structure. Phonon dispersion calculations and first-principles *ab initio* molecular dynamics (AIMD) simulations show that *R*-3*m* Li_2BeN_6, *R*32 Li_2MgN_6, and *P*-62*m* Li_2CaN_6 are kinetically and thermodynamically stable. Electronic property analysis reveals that the high stability of *R*-3*m* Li_2BeN_6 arises from the covalent bonding within the chair-like N_6^{6-} rings. Electronic structure analysis shows that *R*-3*m* Li_2BeN_6 exhibits semiconducting properties, while *R*32 Li_2MgN_6 and *P*-62*m* Li_2CaN_6 exhibit metallic behavior. The unique chair-like N_6^{6-} ring in *R*-3*m* Li_2BeN_6 confers superior energetic characteristics compared to *R*32 Li_2MgN_6 and *P*-62*m* Li_2CaN_6. The theoretical energy density of *R*-3*m* Li_2BeN_6 is 4.38 kJ/g, indicating its potential as a HEDM.

2. Computational details

Structural predictions for the Li_2XN_6 (X = Be, Mg, Ca) systems were performed using the particle swarm optimization (PSO) method implemented in the CALYPSO code.[39,40] This method does not rely on any pre-set structural information and has been successfully validated in various systems, including binary and ternary systems, under high-pressure conditions. Structure optimization and electronic property calculations were performed within the framework of density functional theory (DFT).[41] The Perdew–Burke–Ernzerhof (PBE) generalized gradient approximation (GGA) was employed.[41–43] A Monkhorst–Pack k-mesh with a spacing of $2\pi \times 0.03$ Å^{-1} was used for Brillouin zone sampling, and a plane-wave energy cutoff of 500 eV was applied.[44] Additionally, the supercell method implemented in the PHONOPY code[45] was used to calculate phonon dispersion curves to determine dynamic stability. The NVT (canonical ensemble) was employed for AIMD simulations,[46] where *R*-3*m* Li_2BeN_6 and *R*32 Li_2MgN_6 were simulated in $3 \times 3 \times 3$ supercells, and *P*-62*m* Li_2CaN_6 was simulated in a $4 \times 2 \times 2$ supercell. Each AIMD simulation lasted 10 ps with a time step of 1 fs. The electron localization function (ELF)[46] was used to analyze bonding characteristics and electron localization. Charge transfer analysis was conducted using the Bader program.[47,48]

3. Results and discussion

3.1. Crystal structure

The ternary phase diagrams of Li_2XN_6 (X = Be, Mg, Ca) at pressures of 0–100 GPa were determined through a comprehensive search for stable crystalline structures. The thermodynamic stability and synthesis pathways of Li_2BeN_6, Li_2MgN_6, and Li_2CaN_6 were evaluated by constructing the convex hull using elemental solids (Li, Be/Mg/Ca, N) and all competing binary compounds as reference phases (Figs. 1(a)–1(c)). This provides theoretical support for understanding their stability under high pressure. The formation enthalpies of these ternary nitrides relative to their decomposition products were calculated as a function of pressure, as shown in Fig. 2. Li_2BeN_6 becomes thermodynamically stable above 25 GPa and remains stable beyond 50 GPa, consistent with the phonon calculations presented in the following section (Fig. 2(a)). In contrast, Li_2MgN_6 is metastable at ambient pressure but stabilizes above 1 GPa (Fig. 2(b)). Li_2CaN_6 exhibits negative formation enthalpies relative to a mixture of Ca_3N_2, Li_3N, and N_2 across the entire 0–100 GPa range (Fig. 2(c)), demonstrating its thermodynamic stability throughout the investigated pressure range.

Based on a systematic structural search and optimization of the Li_2XN_6 (X = Be, Mg, Ca) systems, three thermodynamically stable crystal structures were identified, as shown in Figs. 3(a), 3(c), and 3(d). For Li_2BeN_6, the most stable phase is a cage-like structure crystallizing in the *R*-3*m* space group (Fig. 3(a)), which exhibits the lowest energy at 50 GPa. A

distinctive feature of this phase is a chair-shaped N_6^{6-} ring located at its center (Fig. 3(b)), with N–N bond lengths of 1.37 Å and bond angles of 116.97°. Compared to boat-shaped[53] and planar configurations,[54] the chair-form N_6^{6-} ring displays bond angles closer to the ideal value of 120°, reducing electron cloud overlap and Coulomb repulsion, thereby lowering the total energy and enhancing stability. In contrast, Li_2MgN_6 (Fig. 3(c)) and Li_2CaN_6 (Fig. 3(d)) exhibit different nitrogen connection patterns. Li_2MgN_6 adopts a cage-like structure with an *R*32 space group, featuring a three-dimensional enclosed inner cavity formed by Li and N atoms at the center of the structure, whereas Li_2CaN_6 crystallizes in a layered *P*-62*m* structure and does not contain a cavity. Notably, N_6^{6-} rings are absent in these two compounds. The Li–N distances in Li_2BeN_6, Li_2MgN_6, and Li_2CaN_6 are 2.60 Å, 2.20 Å, and 2.20 Å, respectively. Meanwhile, the Be–N, Mg–N, and Ca–N bond lengths increase from 1.86 Å to 2.19 Å and 2.46 Å, consistent with the increasing atomic radii of Be, Mg, and Ca. This trend suggests that from Be to Mg to Ca, the nitrogen polymerization modes and overall structural frameworks evolve accordingly. The detailed crystallographic parameters of all three compounds are listed in Table 1.

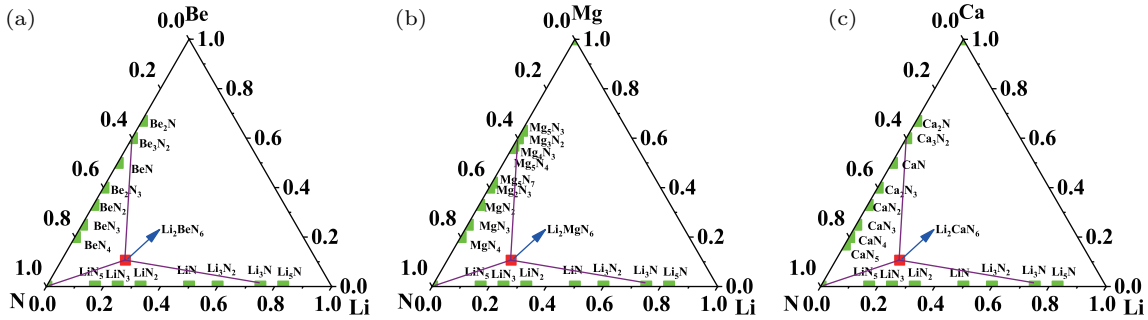


Fig. 1. (a) Ternary phase diagram of Li_2BeN_6 at 50 GPa. (b) Ternary phase diagram of Li_2MgN_6 at 0 GPa. (c) Ternary phase diagram of Li_2CaN_6 at 0 GPa. Pure elemental Li, Be, Mg, Ca, and N, optimized at their respective pressures, were used to construct the convex hull. Binary lithium nitrides (LiN_5, LiN_3, LiN_2, LiN, Li_3N_2, Li_3N, and Li_5N), beryllium nitrides (BeN_4, BeN_3, BeN_2, Be_2N_3, BeN, Be_3N_2, and Be_2N), magnesium nitrides (MgN_4, MgN_3, MgN_2, Mg_2N_3, Mg_5N_7, Mg_5N_4, Mg_4N_3, Mg_3N_2, and Mg_5N_3), and calcium nitrides (CaN_5, CaN_4, CaN_3, CaN_2, Ca_2N_3, CaN, Ca_3N_2, and Ca_2N) were optimized at their corresponding pressures.[49–52]

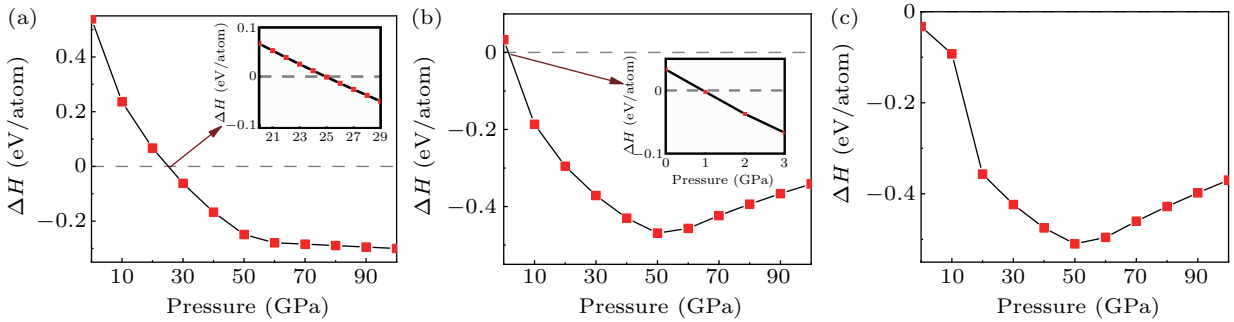


Fig. 2. (a) Enthalpy difference of Li_2BeN_6 relative to a mixture of Be_3N_2, Li_3N, and N_2. (b) Enthalpy difference of Li_2MgN_6 relative to a mixture of Mg_3N_2, Li_3N, and N_2. (c) Enthalpy difference of Li_2CaN_6 relative to a mixture of Ca_3N_2, Li_3N, and N_2.

Table 1. Detailed structural information of Li_2BeN_6, Li_2MgN_6, and Li_2CaN_6 under selected pressures.

Structure	Pressure (GPa)	Lattice parameters	Wyckoff position	Atomic coordinates (fractional)
Li_2BeN_6	50	$a=b=c=3.763$ Å	6*c*	Li (0.000, 0.000, −0.704)
			3*a*	Be (0.000,0.000,0.000)
		$\alpha=\beta=\gamma=81.131°$	18*h*	N (0.159, −0.159, −0.484)
Li_2MgN_6	0	$a=b=c=4.964$ Å	6*c*	Li (0.000, 0.000, 0.335)
			3*a*	Mg (0.000, 0.000, 0.000)
		$\alpha=\beta=\gamma=61.508°$	18*f*	N (−0.001, 0.339, 0.550)
Li_2CaN_6	0	$a=b=5.271$ Å, $c=4.088$ Å	2*c*	Li (0.333, 0.667, 0.000)
			1*a*	Ca (0.000, 0.000, 0.000)
		$\alpha=\beta=90.0°$, $\gamma=120°$	6*i*	N (0.000, 0.377, 0.646)

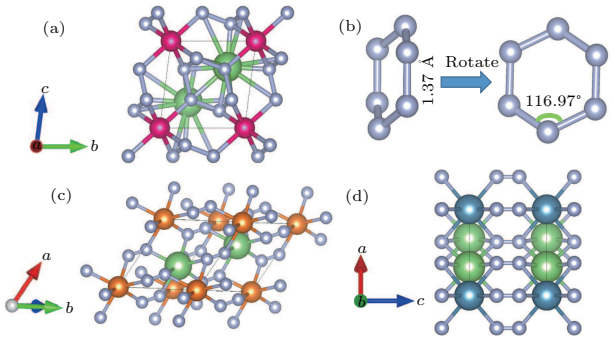


Fig. 3. (a) Crystal structure of Li_2BeN_6 at 50 GPa (green, red, and gray spheres represent Li, Be, and N atoms, respectively). (b) Isolated N_6^{6-} ring structure in Li_2BeN_6. (c) Crystal structure of Li_2MgN_6 at 0 GPa (green, orange, and gray spheres represent Li, Mg, and N atoms, respectively). (d) Crystal structure of Li_2CaN_6 at 0 GPa (green, blue, and gray spheres represent Li, Ca, and N atoms, respectively).

3.2. Kinetic and thermal stability

To determine the kinetic stability of Li_2BeN_6, Li_2MgN_6, and Li_2CaN_6, the phonon spectra were calculated using the supercell method,[55] as shown in Fig. 4. No imaginary frequencies were observed across the entire Brillouin zone at the investigated pressures. This confirms that Li_2MgN_6 and Li_2CaN_6 are dynamically stable at ambient pressure. However, Li_2BeN_6 exhibits dynamical stability only at 50 GPa, adopting a cage structure containing N_6^{6-} rings, which is challenging to stabilize at ambient pressure. Phonon spectrum calculations (supplementary material, Fig. S1) indicate that at 30 GPa and 40 GPa, Li_2BeN_6 exhibits imaginary frequencies in the Brillouin zone, reflecting its dynamical instability at these pressures.

The AIMD simulations were performed to evaluate the thermal stability of Li_2BeN_6, Li_2MgN_6, and Li_2CaN_6 at 300 K, as shown in Fig. 5. The total energy and temperature of the system showed significant oscillations during the initial stage of the simulation, resulting from atomic thermal motion and kinetic–potential energy interchange. The overall trends gradually converge, indicating that the system reaches an equilibrium state. The inset shows the structural evolution from the initial configuration to the final equilibrium state after 10 ps, demonstrating structural stability under the simulated conditions. To further assess thermal and dynamical stability, additional simulations were performed at higher temperatures. The temperature profiles of Li_2BeN_6, Li_2MgN_6, and Li_2CaN_6 (supplementary material, Fig. S2) indicate that Li_2BeN_6, Li_2MgN_6, and Li_2CaN_6 remain stable up to 2500 K, 1500 K, and 500 K, respectively. Chemical bond breaking in Li_2BeN_6, Li_2MgN_6, and Li_2CaN_6 occurs beyond these temperatures (supplementary material, Figs. S3–S5), suggesting that their structural stability is compromised at elevated temperatures.

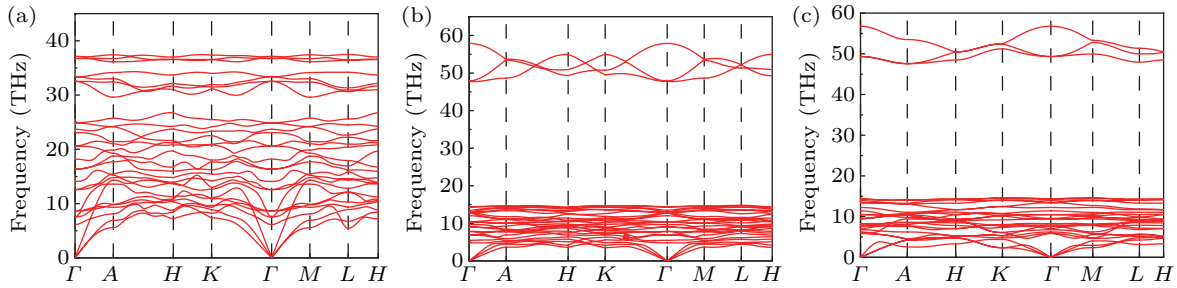


Fig. 4. (a) Phonon spectrum of Li_2BeN_6 at 50 GPa. (b) Phonon spectrum of Li_2MgN_6 at 0 GPa. (c) Phonon spectrum of Li_2CaN_6 at 0 GPa.

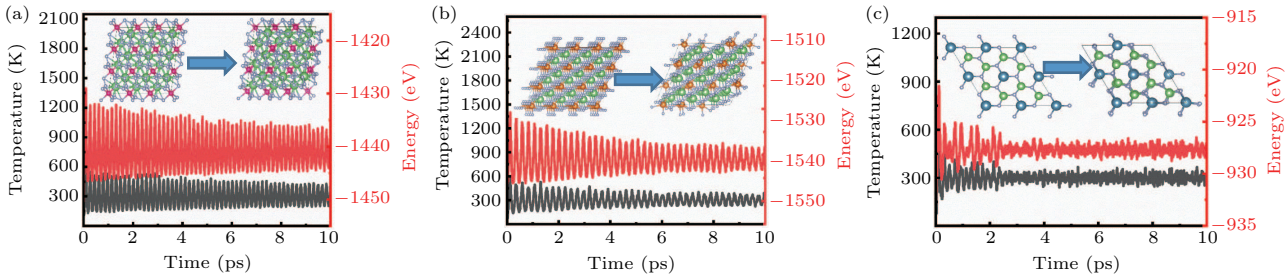


Fig. 5. Temperature and total energy of Li_2BeN_6, Li_2MgN_6, and Li_2CaN_6 during AIMD simulations at 300 K. (a) Li_2BeN_6 at 50 GPa. (b) Li_2MgN_6 at 0 GPa. (c) Li_2CaN_6 at 0 GPa.

3.3. Electronic properties

To explore intrinsic electronic properties, the electronic band structures and projected density of states (PDOS) of Li_2BeN_6, Li_2MgN_6, and Li_2CaN_6 were calculated, as shown in Fig. 6. Li_2BeN_6 exhibits semiconducting behavior with a bandgap of 0.45 eV, whereas Li_2MgN_6 and Li_2CaN_6 display metallic properties. It should be noted that the PBE functional typically underestimates band gaps. The PDOS plots in Figs. 6(a)–6(c) show that within the energy range from −6 eV to 0 eV and near the Fermi level, the density of states is primarily contributed by N 2p orbitals, with weaker contributions

from Li and Be/Mg/Ca s orbitals. To further understand chemical bonding, Bader charge transfer was calculated, as shown in Table 2. As the common cation in the Li_2XN_6 (X = Be, Mg, Ca) compounds, Li exhibits consistent Bader charges of approximately -0.850 $|e|$/atom, indicating its stable electron-donating behavior. In contrast, the central metal atoms exhibit decreasing Bader charges from Be (-1.709 $|e|$) to Mg (-1.612 $|e|$) to Ca (-1.426 $|e|$), indicating a gradual reduction in the electron-accepting ability of nitrogen from Li_2BeN_6 to Li_2MgN_6 and Li_2CaN_6. The analysis indicates that ionic interactions play a crucial role in stabilizing these compounds: in Li_2BeN_6, ionic interactions occur among Li atoms, Be atoms, and the N_6^{6-} ring, while in Li_2MgN_6 and Li_2CaN_6, ionic interactions exist among Li, Mg/Ca, and N atoms.

Table 2. Bader charge analysis results for Li_2BeN_6 at 50 GPa and Li_2MgN_6, Li_2CaN_6 at 0 GPa. Positive values represent electron loss, and negative values represent electron gain; the charge transfer value corresponds to the total charge of all atoms of the same type.

Structure	Pressure (GPa)	Atom	Charge ($\|e\|$)
Li_2BeN_6	50	Li	1.698
		Be	1.709
		N	−3.407
Li_2MgN_6	0	Li	1.751
		Mg	1.612
		N	−3.363
Li_2CaN_6	0	Li	1.741
		Ca	1.426
		N	−3.167

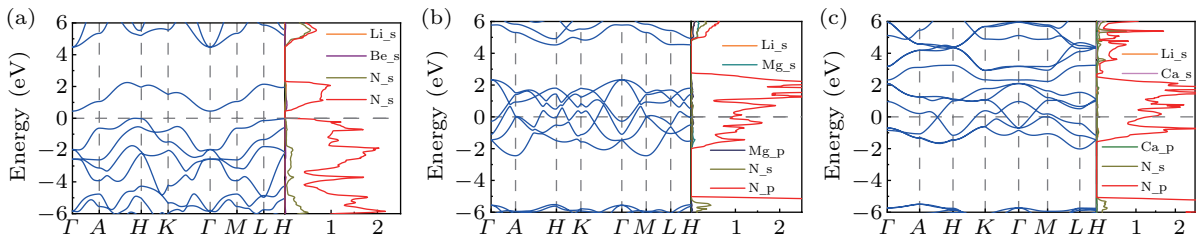


Fig. 6. Electronic properties of Li_2BeN_6, Li_2MgN_6, and Li_2CaN_6. (a) Band structure and PDOS of Li_2BeN_6 at 50 GPa. (b) Band structure and PDOS of Li_2MgN_6 at 0 GPa. (c) Band structure and PDOS of Li_2CaN_6 at 0 GPa.

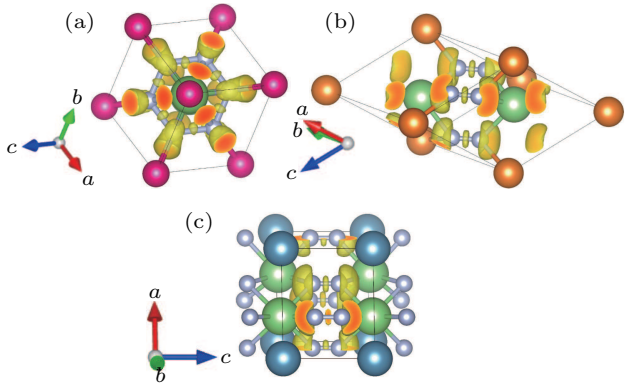


Fig. 7. Three-dimensional ELF of Li_2XN_6 (X = Be, Mg, Ca). (a) Li_2BeN_6 at 50 GPa (green, red, and gray atoms represent Li, Be, and N, respectively; isosurface value = 0.8). (b) Li_2MgN_6 at 0 GPa (green, orange, and gray atoms represent Li, Mg, and N, respectively; isosurface value = 0.8). (c) Li_2CaN_6 at 0 GPa (green, blue, and gray atoms represent Li, Ca, and N, respectively; isosurface value = 0.8).

To characterize the chemical bonds of Li_2BeN_6, Li_2MgN_6, and Li_2CaN_6, the electron localization function (ELF) was calculated, as shown in Fig. 7. In Li_2BeN_6, the N_6^{6-} ring exhibits classical covalent bonding between nitrogen atoms (Fig. 7(a)), while metal cations interact with the N_6^{6-}, contributing to the high structural stability of the compound. As shown in Figs. 7(b) and 7(c), the nitrogen-nitrogen bonds in Li_2MgN_6 and Li_2CaN_6 exhibit localized electrons, confirming their covalent nature. The charge density difference plots for Li_2BeN_6, Li_2MgN_6, and Li_2CaN_6 are presented in Fig. 8, where blue regions represent electron loss and yellow regions represent electron accumulation. It can be observed that nitrogen atoms gain electrons, consistent with Bader charge analysis,[56] and significant electron accumulation between nitrogen atoms indicates covalent N–N bonding, further confirming the stability and high energy density of Li_2BeN_6. Furthermore, the cage-like structure effectively isolates electron density regions, minimizing electron cloud overlap, as evidenced by the charge density difference plot in Fig. 8(a), where electron accumulation is localized around bonding regions with negligible density between adjacent cages.

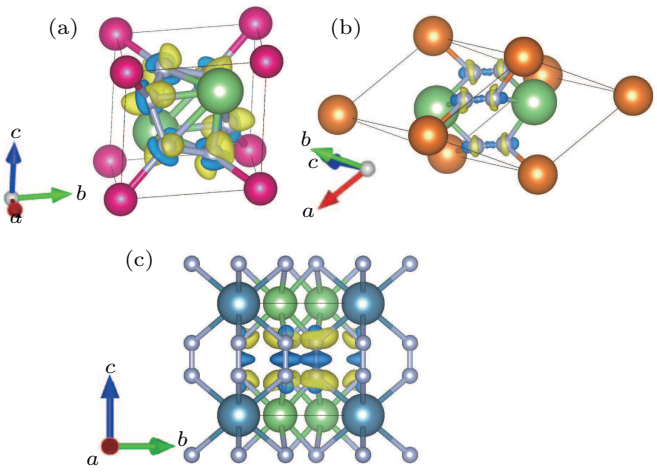


Fig. 8. Schematic diagram of charge density difference. (a) Li_2BeN_6 at 50 GPa (green, red, and gray atoms represent Li, Be, and N, respectively; isosurface value = 0.19). (b) Li_2MgN_6 at 0 GPa (green, orange, and gray atoms represent Li, Mg, and N, respectively; isosurface value = 0.19). (c) Li_2CaN_6 at 0 GPa (green, blue, and gray atoms represent Li, Ca, and N, respectively; isosurface value = 0.19).

Consequently, this spatial confinement of electrons reduces inter-cage repulsion and contributes to the lower total energy of the cage-like Li_2BeN_6 structure. Figures 8(b) and 8(c) show electron transfer from Li, Mg, and Ca to N, suggesting ionic character in the Li–N, Mg–N, and Ca–N bonds.

3.4. Explosive performance

Energy density is a crucial parameter for evaluating the detonation performance of energetic materials. Here, a large amount of energy is released when the predicted stable Li_2XN_6 phase decomposes into stable X_3N_2 and Li_3N solids, along with N_2 gas, under ambient conditions. The dissociation energy of Li_2XN_6 is calculated according to the following decomposition pathway under ambient conditions:[49,50,57]

$$3Li_2XN_6 \rightarrow X_3N_2\,(s) + 2Li_3N\,(s) + 7N_2\,(g). \quad (1)$$

Here, X (X = Be, Mg, Ca) denotes the metal atom, and the labels '(s)' and '(g)' represent the solid and gas phases, respectively. The density of Li_2XN_6 at 0 GPa is calculated from the relative molecular mass of one Li_2XN_6 formula unit and the corresponding equilibrium volume at 0 GPa. The energy density of Li_2XN_6 is obtained by dividing the released dissociation energy (ΔE) by the mass of Li_2XN_6. The energy density of Li_2BeN_6 is 4.38 kJ/g, which is slightly higher than that of the conventional explosive TNT (4.3 kJ/g). In contrast, the energy densities of Li_2MgN_6 and Li_2CaN_6 are relatively low, with values of 0.24 kJ/g and 0.02 kJ/g, respectively. Therefore, the following discussion focuses on Li_2BeN_6.

The detonation properties of Li_2BeN_6, including the detonation velocity (V_d) and detonation pressure (P_d), are important indicators for assessing its potential as a high-energy-density material (HEDM).[58] The Kamlet–Jacobs empirical equations provide a practical method to estimate V_d and P_d based on characteristic parameters. The expressions for V_d and P_d are[59]

$$V_d = 1.01\left(NM^{0.5}E_d^{0.5}\right)^{0.5}(1+1.3\rho), \quad (2)$$

$$P_d = 15.58\rho^2 NM^{0.5}E_d^{0.5}. \quad (3)$$

Here, N represents the moles of N_2 gas generated per gram of Li_2BeN_6, M is the molar mass of N_2 (28 g/mol), E_d is the chemical detonation energy (kJ/g), and ρ is the density of Li_2BeN_6. The experimental detonation velocity and pressure of TNT (6.90 km/s, 190 GPa) and HMX (9.10 km/s, 393 GPa) have been successfully reproduced using this approach.[60] According to the empirical equations, the estimated detonation velocity and pressure of Li_2BeN_6 are 10.60 km/s and 618 GPa, respectively. These values are approximately 1.5 and 3.3 times higher than those of TNT and about 1.2 and 1.6 times higher than those of HMX. These high predicted detonation parameters indicate the promising potential of Li_2BeN_6 as a high explosive (Table 3).

Table 3. Estimated detonation properties of Li_2BeN_6 using the Kamlet–Jacobs empirical equations, compared with experimental values for conventional explosives TNT and HMX.[59,61,62]

Compounds	ρ (g/cm^3)	E_d (kJ/g)	E_v (kJ/cm^3)	V_d (km/s)	P_d (GPa)
Li_2BeN_6	2.73	4.38	11.93	10.60	618
TNT	1.64	4.30	4.30	6.90	190
HMX	1.90	5.70	10.83	9.10	393

It should be noted that the values for traditional energetic materials (TNT and HMX) are obtained from experimental measurements, whereas the performance parameters of Li_2BeN_6 are derived from first-principles calculations, without accounting for energy losses under practical detonation conditions. Therefore, the actual detonation performance may be lower than the theoretical predictions. Nevertheless, these calculations provide valuable reference data for evaluating its energetic potential.

4. Conclusion

The structures of Li_2BeN_6, Li_2MgN_6, and Li_2CaN_6 were successfully predicted using the PSO algorithm as implemented in CALYPSO combined with first-principles calculations. Kinetic and thermodynamic analyses show distinct pressure-dependent stabilities: Li_2BeN_6 is stable at 50 GPa, while Li_2MgN_6 and Li_2CaN_6 are stable at ambient pressure. These stabilities are attributed to differences in crystal packing and chemical bonding. AIMD simulations indicate that Li_2BeN_6, Li_2MgN_6, and Li_2CaN_6 are thermally stable up to 2500 K, 1500 K, and 500 K, respectively. Furthermore, these compounds exhibit thermodynamic stability at 50 GPa, 0 GPa, and 0 GPa, respectively. Notably, Li_2BeN_6 demonstrates potential applications in extreme high-temperature environments. In terms of electronic properties, Li_2BeN_6 is a semiconductor with a band gap of 0.45 eV, whereas Li_2MgN_6 and Li_2CaN_6 exhibit metallic properties. This behavior is related to electron distribution characteristics caused by cation radii and electronegativity. The smaller ionic radius and higher electronegativity of Be^{2+} result in a more localized electron distribution in the N_6^{6-} ring, leading to a finite band gap. In contrast, the larger Mg^{2+} and Ca^{2+} cations delocalize electrons in the lattice, resulting in metallic conductivity. Notably, Li_2BeN_6 shows great potential as a HEDM. Under ambient pressure, it releases 4.38 kJ/g upon decomposition into Li_3N, Be_3N_2, and N_2, with detonation velocity and pressure approximately 1.5 and 3.3 times higher than those of TNT, respectively. This high energy release is attributed to the high bond energy of the N_6^{6-} ring, consistent with the strong covalent bonding observed in charge analysis.

Acknowledgments

This work was supported by the National Natural Science Foundation of China (Grant No. 11774128) and the

Natural Science Foundation of Shandong Province (Grant Nos. ZR2020QA061, ZR2023QA052, ZR2024QA144, and ZR2025QC1496).

References

[1] Zhang J, Niu C, Zhang H, Zhao J, Wang X and Zeng Z 2021 *J. Phys. Chem. Lett.* **12** 5731
[2] Liu L, Qi J, Wang D, Yuan J, Shi D, Xiong Z, Ye T, Cai Y and Zhang L 2025 *Nano Materials* **15** 249
[3] Eremets M I, Gavriliuk A G, Trojan I A, Dzivenko D A and Boehler R 2004 *Nat. Mater.* **3** 558
[4] Li Y, Feng X, Liu H, Hao J, Redfern S A, Lei W, Liu D and Ma Y 2018 *Nat. Commun.* **9** 722
[5] Emery N, Hérold C, d'Astuto M, Garcia V, Bellin C, Marêché J, Lagrange P and Loupias G 2005 *Phys. Rev. Lett.* **95** 087003
[6] Liu Z, Li D, Wei S, Wang W, Tian F, Bao K, Duan D, Yu H, Liu B and Cui T 2017 *Inorg. Chem.* **56** 7494
[7] Zhang S, Zhao Z, Liu L and Yang G 2017 *J. Power Sources* **365** 155
[8] Li X, Zhang S, Zhang C and Wang Q 2018 *Nanoscale* **10** 949
[9] Li J, Jiang Q, Zhu Z, Zhu H and Wang X 2019 *Europhys. Lett.* **124** 67004
[10] Lin J, Zhu Z, Jiang Q, Guo S, Li J, Zhu H and Wang X 2019 *AIP Adv* **9** 055116
[11] Zhu M, Li Q, Zhang L, Su J, Yang C and Wang H 2024 *J. Phys. Chem. Solids.* **191** 112054
[12] Wei S, Li D, Liu Z, Li X, Tian F, Duan D, Liu B and Cui T 2017 *Phys. Chem. Chem. Phys.* **19** 9246
[13] Xia K, Zheng X, Yuan J, Liu C, Gao H, Wu Q and Sun J 2019 *J. Phys. Chem. C* **123** 10205
[14] Wang M and Han D 2022 *ACS Omega* **7** 10812
[15] Li B, Qi H, Duan Y and Peng M 2023 *Mater. Sci. Semicond. Process.* **160** 107400
[16] Liu Z, Li D, Liu Y, Cui T, Tian F and Duan D 2019 *Phys. Chem. Chem. Phys.* **21** 12029
[17] Du H, Ge Y, Zhu J, Guo W and Yao Y 2021 *Phys. Chem. Chem. Phys.* **23** 12350
[18] Guo S-T, Xu Z-Z, Geng Y-L and Rui Q 2023 *Chin. Phys. B* **32** 126202
[19] Bykov M, Bykova E, Aprilis G, Glazyrin K, Koemets E, Chuvashova I, Kupenko I, McCammon C, Mezouar M and Prakapenka V 2018 *Nat. Commun.* **9** 2756
[20] Jiao F, Zhang C and Xie W 2020 *J. Phys. Chem. C* **124** 19953
[21] Sun C, Guo W and Yao Y 2022 *Chin. Phys. Lett.* **39** 087101
[22] Li J, Sun L, Wang X, Zhu H and Miao M 2018 *J. Phys. Chem. C* **122** 22339
[23] Yi W, Zhao K, Wang Z, Yang B, Liu Z and Liu X 2020 *ACS Omega* **5** 6221
[24] Azouaoui A, Hourmatallah A, Benzakour N, Bouslykhane K and Rezzouk A 2022 *Phase Transit* **95** 225
[25] Liu Z, Li D, Tian F, Duan D, Li H and Cui T 2020 *Inorg. Chem.* **59** 8002
[26] Shi X, Yao Z and Liu B 2020 *J. Phys. Chem. C* **124** 4044
[27] Xin S, Du D, Wang F, Rui Q, Wang Q, Zhao X, Li J, Yang D, Zhu H and Wang X 2021 *Physica B* **617** 413139
[28] Murtaza G, Haseeb M, Javed A, Rafiq M, Rasul M and Hussain A 2024 *Mater. Sci. Semicond. Process.* **176** 108354
[29] Guo S, Lin J, Li J, Wang Q, Wu H, Zhu H and Wang X 2019 *Comput. Mater. Sci.* **169** 109147
[30] Mukkavilli R S, Moharana N, Singh B, Fischer T, Vollnhals F, Ichangi A, Kumar K H, Christiansen S, Kim K H and Kwon S 2024 *Nano Energy* **129** 110046
[31] Salke N P, Xia K, Fu S, Zhang Y, Greenberg E, Prakapenka V B, Liu J, Sun J and Lin J F 2021 *Phys. Rev. Lett.* **126** 065702
[32] Wang X, Li J, Botana J, Zhang M, Zhu H, Chen L, Liu H, Cui T and Miao M 2013 *J. Chem. Phys.* **139** 164710
[33] Zhang M, Yin K, Zhang X, Wang H, Li Q and Wu Z 2013 *Solid State Commun.* **161** 13
[34] Babu K R and Vaitheeswaran G 2012 *Chem. Phys. Lett.* **533** 35
[35] Etourneau J, Portier J and Ménil F 1992 *J. Alloys Compd.* **188** 1
[36] Somer M, Carrillo-Cabrera W, Peters E-M, Peters K and Von Schnering H 1996 *Z. Krist. Cryst. Mater.* **211** 635
[37] Juza R and Hund F 1946 *Naturwissenschaften* **33** 121
[38] Cordier G, Gudat A, Kniep R and Rabenau A 1989 *Angew. Chem. Int. Ed.* **28** 1702
[39] Wang Y, Lv J, Zhu L and Ma Y 2012 *Comput. Phys. Commun.* **183** 2063
[40] Wang Y, Lv J, Zhu L and Ma Y 2010 *Phys. Rev. B* **82** 094116
[41] Grimme S, Antony J, Ehrlich S and Krieg H 2010 *J. Chem. Phys.* **132** 154104
[42] Grimme S, Ehrlich S and Goerigk L 2011 *J. Comput. Chem.* **32** 1456
[43] Perdew J P, Burke K and Ernzerhof M 1996 *Phys. Rev. Lett.* **77** 3865
[44] Monkhorst H and Pack J 1977 *Phys. Rev. B* **16** 1748
[45] Togo A and Tanaka I 2015 *Scr. Mater.* **108** 1
[46] Becke A D and Edgecombe K E 1990 *J. Chem. Phys.* **92** 5397
[47] Yang Y and Coppens P 1978 *Found. Crystallogr.* **34** 61
[48] Henkelman G, Arnaldsson A and Jónsson H 2006 *Comput. Mater. Sci* **36** 354
[49] Shen Y, Oganov A R, Qian G, Zhang J, Dong H, Zhu Q and Zhou Z 2015 *Sci. Rep.* **5** 14204
[50] Wei S, Li D, Liu Z, Wang W, Tian F, Bao K, Duan D, Liu B and Cui T 2017 *J. Phys. Chem. C* **121** 9766
[51] YU SY H B and Zeng Q 2017 *J. Phys. Chem. C* **121** 11037
[52] Zhu S, Peng F, Liu H, Majumdar A, Gao T and Yao Y 2016 *Inorg. Chem.* **55** 7550
[53] Prasad D L, Ashcroft N and Hoffmann R 2013 *J. Phys. Chem. C* **117** 20838
[54] Zhang M, Yan H, Wei Q, Wang H and Wu Z 2013 *Europhys. Lett.* **101** 26004
[55] Monkhorst H J and Pack J D 1976 *Phys. Rev. B* **13** 5188
[56] Tang W, Sanville E and Henkelman G 2009 *J. Phys.:Condens. Mat.* **21** 084204
[57] Pickard C J and Needs R 2009 *Phys. Rev. Lett.* **102** 125702
[58] Geith J, Klapötke T M, Weigand J and Holl G 2004 *Propellants. Explos. Pyrotech.* **29** 3
[59] Kamlet M J and Dickinson C 1968 *J. Chem. Phys.* **48** 43
[60] Wang Y, Liu Y, Song S, Yang Z, Qi X, Wang K, Liu Y, Zhang Q and Tian Y 2018 *Nat. Commun.* **9** 2444
[61] Hu Y, Huang P, Guo L, Wang X and Zhang C 2006 *Phys. Lett. A* **359** 728
[62] Kamlet M J and Jacobs S 1968 *J. Chem. Phys.* **48** 23